Materials
Advances

Accepted Manuscript

This article can be cited before page numbers have been issued, to do this please use: H. Icil, P. Karsili, M. Dinleyici, J. Tohtayeva, S. Altnk and S. Koyuncu, *Mater. Adv.*, 2026, DOI: 10.1039/D6MA00426A.

View Article Online
DOI: 10.1039/D6MA00426A

Novel perylene-bridged polyethyleneimine polymer networks: synthesis and photophysical–electrochemical insights for supercapacitor applications

Huriye Icil[a,*], Pelin Karsili[a], Meltem Dinleyici[a], Jahan Tohtayeva[b], Sinem Altınışık[c], Sermet Koyuncu[c,*]

[a]Department of Chemistry, Faculty of Arts and Sciences, Eastern Mediterranean University, 99628, Famagusta, N. Cyprus, Mersin 10, Turkey

[b]Department of Energy Resources and Management, Canakkale Onsekiz Mart University, 17100, Canakkale, Turkey

[c]Department of Chemical Engineering, Faculty of Engineering, Canakkale Onsekiz Mart University, 17100, Canakkale, Turkey

ABSTRACT

In this work, we introduce a molecular design strategy to construct nitrogen-rich, π-conjugated, redox-active polymer networks using perylene-3,4,9,10-tetracarboxylic dianhydride as a multifunctional cross-linker for branched polyethyleneimine (PEI) for the first time. Two novel PEI–perylene networks, PEI-3 and PEI-5, were synthesised through imidization between the anhydride groups of the perylene precursor and the amine functionalities of PEI with molecular weights of 60 kDa and 25 kDa, respectively. The resulting insoluble networks combine PEI-derived nitrogen-rich domains with redox-active perylene imide/carbonyl units and π–π interacting conjugated segments. Structural, optical, morphological, thermal, and electrochemical properties were investigated using ^{1}H NMR, FTIR, Raman, UV–visible and fluorescence spectroscopy, SEM, EDX, XPS, TEM, and TGA analyses. Spectroscopic results confirmed perylene incorporation and imide-linked network formation, while optical studies revealed characteristic perylene-based absorption/emission features and aggregation-related photophysical behavior. Electrochemical measurements showed that polymer architecture strongly influences charge-storage behavior. PEI-3 exhibited higher specific capacitance and better capacitance retention than PEI-5, retaining approximately 83% of its initial capacitance after 3000 charge–discharge cycles, whereas PEI-5 showed lower capacitance but a more compact network architecture and enhanced thermal robustness. A PEI-3 symmetric supercapacitor device further delivered a specific capacitance of 107 F g^{-1} at 1 A g^{-1}, a maximum energy density of 43 Wh kg^{-1} at a power density of 850.7 W kg^{-1}, and 81% capacitance retention after 4000 cycles. These findings establish perylene dianhydride cross-linking as a promising route to metal-free, redox-active organic electrode materials for advanced supercapacitors.

KEYWORDS
Perylene-crosslinked polyethylenimine · Photophysical properties · Electrochemical performance · Supercapacitor materials · Energy storage

---

* Corresponding authors.

orcid.org/0000-0002-3389-6734; *E-mail address:* huriye.icil@emu.edu.tr (H. Icil)

View Article Online
DOI: 10.1039/D6MA00426A

1. Introduction

The challenges posed by climate change and the growing global demand for energy have intensified the need for cleaner and more sustainable energy technologies [1]. As the transition away from fossil fuels accelerates, the integration of renewable energy sources such as solar and wind into modern energy systems has become increasingly important [2,3]. However, the intermittent nature of these renewable resources requires efficient and reliable energy storage technologies, positioning electrochemical energy storage devices as key components of sustainable energy infrastructures. In parallel, the rapid expansion of portable electronics, electric vehicles, wearable devices, and smart-grid technologies has increased demand for high-power, long-life energy storage systems. Recent market analyses estimate that the global supercapacitor market was valued at approximately USD 2.9 billion in 2024 and is projected to reach around USD 15.3 billion by 2034, highlighting the growing commercial relevance of fast and durable energy storage technologies [4].

Among electrochemical energy storage devices, supercapacitors have attracted considerable attention owing to their high power density, long cycle life, rapid charge–discharge capability, and excellent operational stability [5–10]. Nevertheless, their relatively low energy density compared with batteries remains a major limitation. Consequently, significant research efforts have focused on improving electrode materials by introducing pseudocapacitive behaviour via fast, reversible Faradaic processes [11–13]. In the broader field of advanced nanomaterials and sustainable technologies, several material classes, including defect-engineered metal oxides, heterostructured nanosystems, MXenes, metal sulfide photocatalysts, and green nanoscale semiconductors, have demonstrated the importance of controlling composition, dimensionality, defects, heterointerfaces, and charge-transfer pathways for energy conversion, energy storage, and environmental applications [14–17]. These developments show that nanoscale structural engineering can significantly improve charge transport, ion accessibility, and interfacial reactivity. However, many inorganic nanomaterial-based systems may face challenges related to metal resource dependence, processing complexity, aggregation or restacking, long-term stability, and scalable integration into lightweight, flexible electrode architectures. Therefore, there remains a clear materials gap for redox-active, structurally tunable, metal-free or low-metal-content polymeric systems that combine ion accessibility with electronically active charge-transport pathways.

Heteroatom-containing organic materials and π-conjugated frameworks have emerged as promising alternatives because they can provide redox-active sites, improve interfacial wettability, and facilitate charge transport within electrode architectures [18–21]. Perylene-based compounds, particularly N,N′-substituted perylene-3,4,9,10-tetracarboxylic diimides, are well-known π-conjugated systems that have been widely explored in optoelectronic and energy-related applications [22–27]. Their extended π-conjugation, high electron affinity, photochemical stability, and reversible redox behaviour make them attractive building blocks for electrochemical energy storage systems [28–34]. Related perylene-containing molecular and polymeric systems have also been investigated for their photophysical behaviour, charge-transfer processes, and functional materials properties, providing an important foundation for the design of perylene-based polymer networks [35–38]. In addition, the rigid aromatic perylene core can promote π–π interactions and electronic communication, which are important for charge transport and redox activity in conjugated electrode materials.

Several perylene/PDI-based electrode architectures, including PDI–carbon composites, PDI-based polymer films, and symmetric or asymmetric supercapacitor systems, have recently been reported for electrochemical energy storage [24–34,41–44]. These studies demonstrate the potential of perylene-based redox-active units in energy-storage electrodes. However, many molecular perylene/PDI-based systems may suffer from aggregation, limited ion accessibility, insufficient electrode integrity, and possible detachment or dissolution during cycling. Therefore, the covalent integration of perylene units into stable polymer networks represents a novel and promising strategy for improving structural robustness while preserving redox and π-conjugated functionality.

Polyethyleneimine (PEI) is a nitrogen-rich polymer containing primary, secondary, and tertiary amine groups, which provide high reactivity and strong interactions with charged or polar species [39,40]. Owing to its structural versatility and high functional group density, PEI has been widely used in adsorption, surface modification, and functional polymer design. From a materials-design perspective, PEI offers several advantages for energy-storage electrodes, including abundant nitrogen-containing sites, chemical reactivity toward anhydrides, and the ability to form cross-linked networks. However, pristine PEI lacks an extended π-conjugated backbone and has limited electronic conductivity, restricting its use as an efficient standalone supercapacitor electrode material. Therefore, integrating PEI with electronically active π-conjugated units is required to improve charge transport, redox functionality, and electrode stability.

To the best of our knowledge, the use of perylene-3,4,9,10-tetracarboxylic dianhydride (PTCDA) as a π-conjugated cross-linking agent for PEI-based polymer networks has not yet been reported. The introduction of this perylene dianhydride unit, therefore, represents a new molecular design strategy that combines the nitrogen-rich, structurally versatile PEI framework with the redox-active, photophysically functional perylene core. Compared with conventional inorganic nanomaterials such as metal oxides, sulfides, and MXenes, the present PEI–perylene networks offer a metal-free organic platform in which molecular structure, cross-link density, ion accessibility, π–π interactions, and redox-active imide/carbonyl units can be tuned through chemical design. This approach addresses the research gap between highly conductive inorganic nanostructures and processable redox-active organic polymer networks for supercapacitor applications.

In this study, we report the synthesis of novel perylene-3,4,9,10-tetracarboxylic dianhydride-cross-linked polyethyleneimine polymer networks using branched PEI precursors with molecular weights of 60 kDa and 25 kDa. In the present design, perylene dianhydride functions as a multifunctional π-conjugated cross-linker that covalently converts branched PEI into insoluble, nitrogen-rich, and electroactive polymer networks. The resulting architecture integrates redox-active perylene imide units, π–π interactions, PEI-derived nitrogen-containing domains, and improved structural integrity. From a practical perspective, the solution-processable synthesis and simple electrode fabrication route provide an initial basis for scalable preparation and reproducible electrode construction. At the same time, the cycling and rate-performance analyses offer preliminary insight into operational stability. The electrochemical performance is further benchmarked against reported perylene/PDI-based supercapacitor systems and compared with conventional carbon-based electrode materials. Overall, this work establishes a structure–property–performance relationship between π-conjugated cross-linking, polymer network morphology, aggregation behaviour, and electrochemical charge storage, providing new insight into the design of functional organic polymer networks for advanced energy-storage systems.

View Article Online
DOI: 10.1039/D6MA00426A

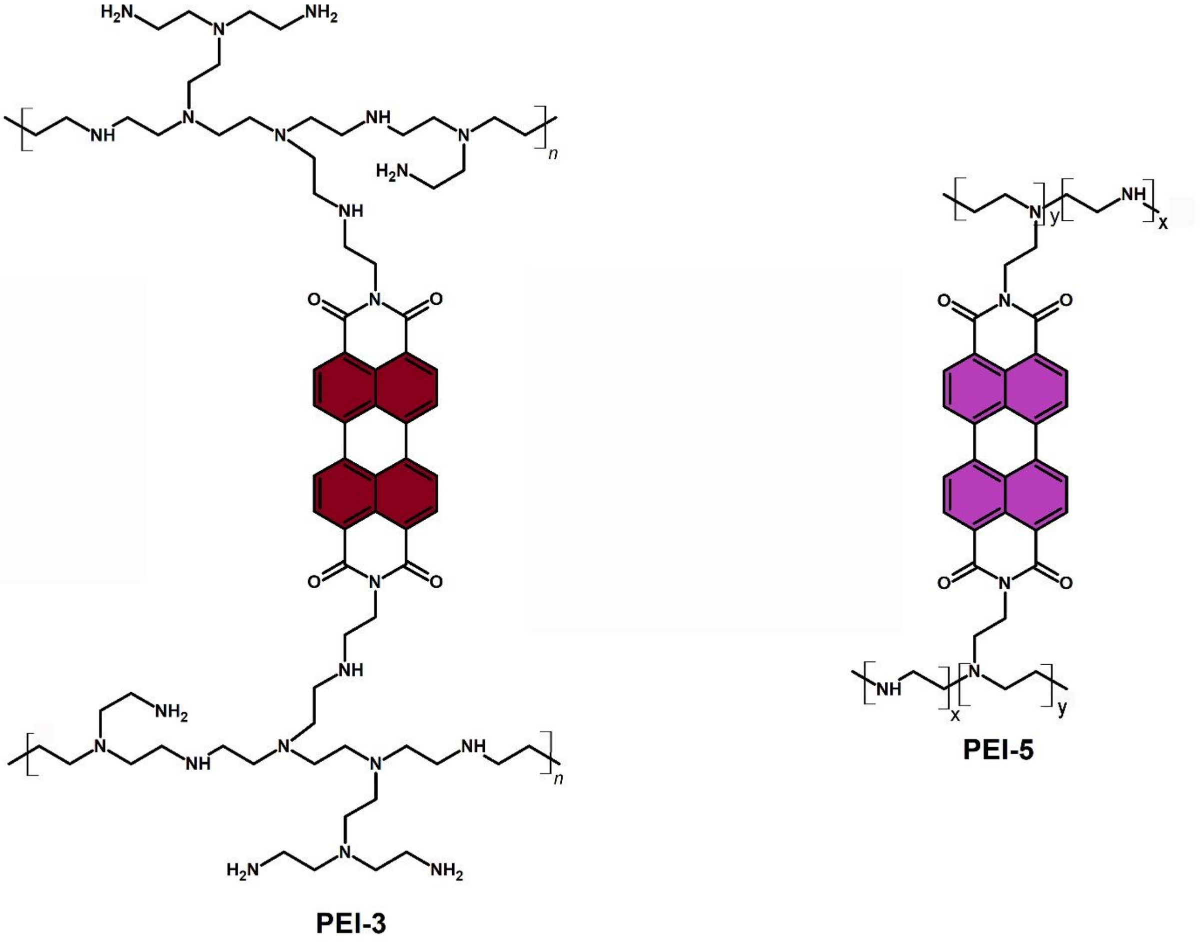

Fig. 1 Proposed structures of the perylene-cross-linked polyethyleneimine networks PEI-3 and PEI-5.

View Article Online
DOI: 10.1039/D6MA00426A

2. Experimental section

2.1. Materials and characterisation

Perylene-3,4,9,10-tetracarboxylic dianhydride (1), branched polyethyleneimines (PEI; average molecular weights of 60 kDa (2) and 25 kDa (4)), m-cresol, and isoquinoline were purchased from Sigma-Aldrich and used as received unless otherwise stated. Before use, m-cresol and isoquinoline were dried over activated 4 Å molecular sieves to remove residual moisture. All solvents employed were of spectroscopic grade.

^{1}H NMR spectra were recorded on a Bruker spectrometer operating at 400 MHz using deuterated dimethyl sulfoxide ($(CD_3)_2SO$) as the solvent and tetramethylsilane (TMS) as the internal reference. Fourier-transform infrared (FT-IR) spectra were obtained using a JASCO FT/IR-6200 spectrometer in the range of 500–4000 cm^{-1} with a resolution of 4 cm^{-1}. X-ray photoelectron spectroscopy (XPS) experiments were carried out (Physical Electronics (PHI), Versa Probe 5000) using a Physical Electronics (PHI) Versa Probe 5000 analyzer. The X-ray spot size was carefully calibrated to 100 µm to guarantee accurate measurements. A monochromatic Al Kα X-ray source was employed, functioning at an energy output of 48.3 W. Measurements were performed at a pass energy of 23.50 eV, with an energy-step resolution of 0.1 eV and a dwell time of 200 ms for each measurement. Calibration was carried out using Ag, Au, and Cu standards. Ultraviolet–visible (UV–vis) absorption spectra were recorded on a Varian Cary100 spectrophotometer at room temperature, while fluorescence emission spectra were obtained using a Varian Cary Eclipse fluorescence spectrophotometer. Fluorescence quantum yields (Φ_f) were determined according to previously reported methods [35–38]. Thermogravimetric analysis (TGA) was performed on a PerkinElmer instrument under a nitrogen atmosphere at a heating rate of 10 °C min^{-1}. Morphological analysis was performed using scanning electron microscopy (SEM, JEOL JSM-7100F), and X-ray diffraction (XRD) patterns were recorded on a PANalytical Empyrean diffractometer.

2.2. Electrode preparation and supercapacitor measurements

Cyclic voltammetry (CV) and galvanostatic charge-discharge (GCD) measurements were performed to evaluate supercapacitor performance at different scan rates and current densities. Measurements were conducted over the potential ranges 0.0-1.0 V for the three-electrode system and 0.0-1.7 V for the symmetrical device. Electrochemical impedance spectroscopy (EIS) measurements were performed in the frequency range of 1 MHz to 100 MHz at open-circuit potential. For active electrode preparation, PEI-3 or PEI-5 polymer was mixed with PVDF-HFP binder in acetone to obtain a homogeneous slurry. The resulting slurry was evenly coated onto a graphite substrate and dried at 60 °C for 1 h to remove any remaining solvent. The active material loading on the electrode was adjusted to approximately 2 mg/cm^2. In the symmetrical device architecture, a paper separator moistened with 1 M H_2SO_4 was placed between the electrodes. After surface contact was established, the system was gently pressed and used directly in electrochemical measurements. All electrode fabrication parameters, including slurry composition, coating area, active material loading, and drying conditions, were carefully controlled to ensure reproducibility. In addition, multiple electrodes prepared under identical conditions exhibited consistent electrochemical behavior.

Capacitance values were calculated considering the mass of the coated active material and the geometric surface area of the electrodes. Specific capacitance (C_m, F g^{-1}) was obtained from GCD curves using the standard capacitance calculation equation. The capacitive contributions of the electrodes were evaluated using the Dunn method. In addition, the energy and power density of the device were calculated using the following equations.

Supercapacitor system, the mass-specific capacity is calculated according to the GCD curve using the following equations:

$$C_m = I \times t / m \times \Delta V \quad (1)$$

where C_m is the gravimetric capacitance, m is the mass of active material (2 mg), I is the discharging current (A), t is the discharging time (s) and ΔV is the potential window.

Electrode kinetic analysis is performed by the following equation:

$$i = k_1 \nu + k_2 \nu^{1/2} \quad (2)$$

$$i/\nu^{1/2} = k_1 \nu^{1/2} + k_2 \quad (3)$$

Where i is absolute value of peak current density (A g-1), and ν is the scan rate (mV s-1).

The following equations calculate the energy density and power density of the SC:

$$E = C_m \times \Delta V^2 / 7.2 \quad (4)$$

$$P = E \times 3600 / t \quad (5)$$

Where E is the energy density, and P is the power density, Coulombic efficiency has been calculated as follows:

$$\eta = t_d / t_c \quad (6)$$

View Article Online
DOI: 10.1039/D6MA00426A

Herein, t_d is the discharge time, and t_c is the charge time.

To further investigate the charge-storage kinetics, the b-value was determined according to the following power-law equation:

$$i = a\nu^b \tag{7}$$

$$\log(i)=b\log(\nu)+\log(a) \tag{8}$$

Where i is the current response, ν is the scan rate, and a and b are adjustable parameter.

2.3. Synthesis

2.3.1. Synthesis of perylene cross-linked 60 kDa polyethyleneimine (PEI-3)

In this synthesis, we have used a branched 60 kDa (average M_n ~ 60 000 by GPC, branched) polyethyleneimine from Sigma Aldrich (2, 0.543 g, 1.02 mmol) and perylene-3, 4, 9, 10-tetracarboxylic acid dianhydride (1, 0.4 g, 1.02 mmol) were dissolved entirely in a well-dried solvent mixture (2 mL isoquinoline and 20 mL *m*-cresol) under an inert atmosphere. The resulting red reaction mixture was heated to 120 °C for 4 hours, then to 160 °C for an additional 6 hours to facilitate the desired chemical transformation.

The cross-linking of polyethyleneimine (PEI) can be effectively monitored by Fourier Transform Infrared (FT-IR) spectroscopy, where a shift from characteristic anhydride to imide bands is observed, indicating successful cross-linking (Fig. S2). The resultant cross-linked polymer exhibited a notable colour transition from red to deep purple, serving as a visual indicator of the reaction's progress. Upon reaching ambient temperature, the reaction mixture was slowly added to 300 mL of cold acetone, facilitating the precipitation of the cross-linked polymer. The precipitate was subsequently isolated by vacuum filtration. To remove unreacted monomers and residual high-boiling solvents, a Soxhlet extraction was performed for 48 hours with ethyl acetate. The solid product was dried in a vacuum oven at 100 °C under reduced pressure. Perylene cross-linked 60 kDa polyethyleneimine was obtained as a bordeaux powder (0.613 g, 65% yield).

FTIR (Fig. S2, KBr, thin film, cm^{-1}): 3381 (amine N─H stretch), 2936 and 2828 (aliphatic C─H stretch), 1689 and 1649 (imide C=O stretch), 1592 (aromatic C=C stretch), 1438 and 1344 (imide C-N stretch), 809, 748 and 654 (aromatic C-H bend). **UV-Vis** (Fig. 3, DMF) (λmax / nm): 460, 489, 524. **Fluorescence** (DMF) (λ_{max} / nm): 537, 575, 628. **^{1}H NMR**, (PEI-3, Figs.

View Article Online
DOI: 10.1039/D6MA00426A

S1 and S5, δ_H ppm, 400 MHz, DMSO-d6): 8.01(s, 8H, H-C(25), H-C(26), H-C(29), H-C(30), H-C(31), H-C(32), H-C(35), H-C(36)), 3.36 (s, 96H, H-C(1), H-C(1'), H-C(2), H-C(2'), H-C(3), H-C(3'), H-C(4), H-C(4'), H-C(5), H-C(5'), H-C(6), H-C(6'), H-C(7), H-C(7'), H-C(8), H-C(8'), H-C(9), H-C(9'), H-C(10), H-C(10'), H-C(11), H-C(11'), H-C(12), H-C(12'), H-C(13), H-C(13'), H-C(14), H-C(14'), H-C(15), H-C(15'), H-C(16), H-C(16'), H-C(17), H-C(17'), H-C(18), H-C(18'), H-C(19), H-C(19'), H-C(20), H-C(20'), H-C(21), H C(21'), H-C(22), H-C(22'), H-C(23), H-C(23'), H-C(24),H-C(24').

^{1}H NMR of PEI (60 kDA, 2), (Figs. S1 and S4, δ_H ppm, 400 MHz, DMSO-d6): 3.16, 2.96 (b, NH_2 protons of PEI), 2.40–2.51 (b, CH_2 protons of PEI).

2.3.2. Synthesis of perylene-crosslinked 25 kDa polyethyleneimine (PEI-5)

In this experiment, we used a branched 25 kDa polyethyleneimine (average molecular weight 25,000) sourced from Sigma-Aldrich (St. Louis, MO). A total of 0.162 g (4, 1.02 mmol) of polyethyleneimine and 0.4 g (1, 1.02 mmol) of perylene-3,4,9,10-tetracarboxylic acid dianhydride were introduced into a dry solvent mixture consisting of 2 mL isoquinoline and 20 mL m-cresol, all under an inert atmosphere to prevent moisture and oxidative degradation. The reaction mixture was heated to 120 °C for 4 hours to promote the initial reaction phase, then raised to 160 °C for an additional 6 hours to complete the reaction. This stepwise increase in temperature facilitates optimal reaction kinetics and ensures efficient formation of the desired polymeric structure. Similar to the synthesis with 60 kDa PEI (PEI-3), we have observed a color change from red to deep purple. The end of the cross-linking reaction was monitored using FT-IR spectroscopy. After the reaction was complete, the mixture was cooled to room temperature and then poured into 300 mL of cold ethyl acetate. The precipitate was collected by vacuum filtration. The unreacted reactants and high-boiling solvents were removed using ethyl acetate in a Soxhlet extraction for 2 days. The solid product was dried in a vacuum oven at 100 °C under reduced pressure. Perylene cross-linked 25 kDa polyethyleneimine, PEI-5, was obtained as a dark purple powder (0.506 g, 90 % yield).

Following the methodology established with 60 kDa polyethyleneimine (PEI), we observed a notable colour transition from red to deep purple during synthesis. The progression and completion of the cross-linking reaction were assessed through Fourier Transform Infrared (FT-IR) spectroscopy. Once the reaction had reached completion, the mixture was cooled to ambient temperature before being diluted with 300 mL of cold ethyl acetate, which facilitated precipitate formation. The precipitate was subsequently collected by vacuum

DOI: 10.1039/D6MA00426A

filtration. To eliminate unreacted starting materials and residual high-boiling solvents, a Soxhlet extraction was performed for 48 hours using ethyl acetate. The resulting solid product was dried in a vacuum oven at 100 °C under reduced pressure, yielding a perylene-cross-linked 25 kDa polyethyleneimine as a dark purple powder weighing 0.506 g, corresponding to a 90% yield.

FTIR (Fig. S3, KBr, thin film, cm^{-1}): 3373 (amine N-H stretch), 2932 and 2824 (aliphatic C-H stretch), 1689 and 1649 (imide C=O stretch), 1592 (aromatic C=C stretch), 1438 and 1344 (imide C-N stretch), 809, 744 and 651 (aromatic C-H bend). **UV-Vis** (Fig. 3, DMF) (λ_{max} / nm): 460, 489, 524. **Fluorescence** (DMF) (λ_{max} / nm): 536, 575, 631. **^{1}H NMR**, (Figs. S1 and S7, δ_H ppm, 400 MHz, DMSO-d6,): 8.00 (s, 8H, H-C(7), H-C(8), H-C(11), H-C(12), H-C(13), H-C(14), H-C(17), H-C(18)), 3.36–3.48 (d, 24H, H-C(1), H-C(1’), H-C(2), H-C(2’), H-C(3), H-C(3’), H-C(4), H- C(4’), H-C(5), H-C(5’), H-C(6), H-C(6’).

^{1}H NMR of PEI (25 kDA, 4), (Figs. S1 and S6, δ_H ppm, 400 MHz, DMSO-d6): 2.55, 2.47 (b, and NH_2 protons of PEI), 1.84 (b, CH_2 protons of PEI).

3. Results and discussion

3.1. Synthesis and characterisation of PEI-3 and PEI-5

Two branched, cross-linked polyethyleneimine (PEI) networks (PEI-3 and PEI-5) were successfully synthesised via an imidization reaction using perylene-3,4,9,10 tetracarboxylic dianhydride as a π-conjugated cross-linking agent. To the best of our knowledge, this is the first report of the use of perylene-3,4,9,10-tetracarboxylic dianhydride as a crosslinker in polyethyleneimine-based polymer networks. The two PEI precursors employed in this study possess significantly different molecular weights (60 kDa and 25 kDa), which are expected to influence the resulting network structure, cross-linking density, and ultimately their physicochemical and electrochemical properties.

The imidization reaction proceeds via nucleophilic attack by the primary amine groups of polyethyleneimine on the carbonyl centres of the perylene dianhydride, forming imide linkages with the elimination of water. The successful formation of the cross-linked networks was confirmed by FT-IR spectroscopy, which shows the complete disappearance of the characteristic anhydride absorption band at 1773 cm^{-1} and the emergence of imide-related bands (Fig. S2 and S3). To remove unreacted monomers and residual high-boiling solvents, the crude products were Soxhlet-extracted, yielding purified cross-linked polymer networks.

The formation of the cross-linked polyethyleneimine (PEI) architectures (PEI-3 and PEI-5) was confirmed by Fourier-transform infrared (FT-IR) spectroscopy, XPS and ^{1}H NMR analysis

View Article Online
DOI: 10.1039/D6MA00426A

(Figs. 2 S1–S7). The proposed network structures arise from imidization reactions between the primary amine groups of PEI and the anhydride functionalities of the perylene cross-linker. The presence of primary amines along extended chains is expected to facilitate cross-linking by reducing steric hindrance, although alternative cross-linking sites cannot be ruled out.

FT-IR spectra clearly indicate the successful conversion of the dianhydride into imide structures, as evidenced by the disappearance of the characteristic anhydride band and the appearance of imide-related absorptions, confirming effective cross-linking.

The solubility of PEI-3 and PEI-5 was systematically evaluated in a range of organic solvents (Table S1 and Fig. S8). Both materials exhibit limited solubility in common polar aprotic solvents such as DMF, DMAc, NMP, and DMSO, consistent with their cross-linked network structures. The materials exhibit a characteristic bordeaux colour under ambient light and fluorescence under UV irradiation (365 nm), indicating the presence of perylene-based chromophores. A summary of the solubility behaviour and optical properties is provided in Tables 1 and S1–3.

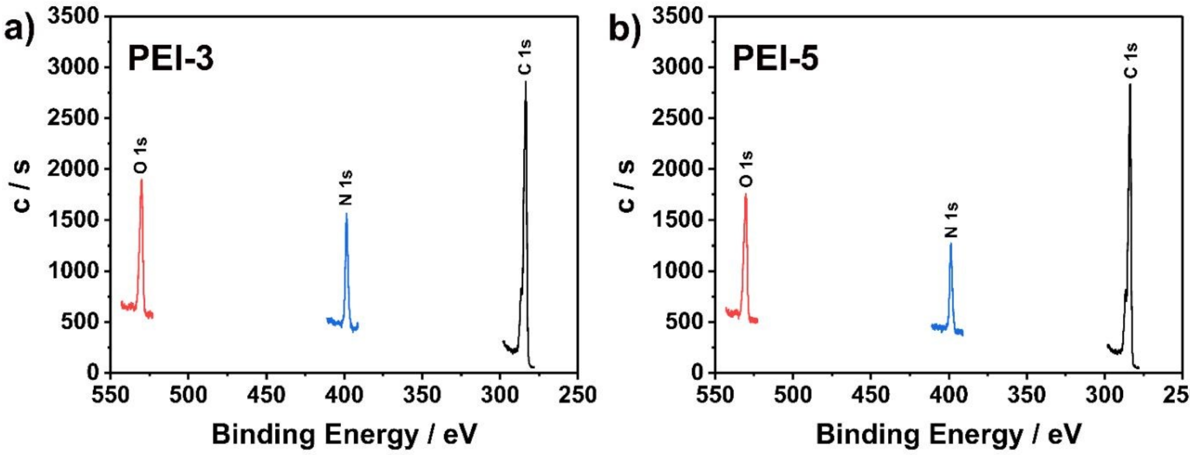

Fig. 2 The high-resolution XPS core-level spectra of (a) PEI-3 and (b) PEI-5, showing the C 1s, N 1s, and O 1s signals associated with the carbon-, nitrogen-, and oxygen-containing functionalities of the PEI–perylene polymer networks.

FT-IR spectroscopy was employed to confirm the formation of cross-linked polyethyleneimine (PEI) networks (PEI-3 and PEI-5) through imidization with perylene-3,4,9,10-tetracarboxylic dianhydride. The spectra of the starting materials and products are shown in Figs. S2 and S3. The FT-IR spectrum of perylene dianhydride exhibits characteristic absorption bands of the anhydride functional group, including strong C=O stretching at 1773 $\mathrm{cm^{-1}}$, aromatic C=C stretching at 1595 $\mathrm{cm^{-1}}$, and C–O–C stretching at 1023 $\mathrm{cm^{-1}}$ (Fig. S2a). In contrast, the spectra of branched polyethyleneimines (60 kDa and 25 kDa) display typical amine-related bands, such as N–H stretching around 3400 cm^{-1}, aliphatic C–H stretching in the range of 2960–2845 cm^{-1}, N–H bending near 1657 cm^{-1}, and C–N stretching bands between 1316 and 1100 cm^{-1} (Figs. S2b and S3b). Following cross linking, significant spectral changes are observed, confirming successful imidization. In particular, the disappearance of the characteristic anhydride bands at 1773 and 1023 cm^{-1}, together with the appearance of imide-related absorptions at approximately 1689 and 1649 cm^{-1}, provides clear evidence for the formation of imide linkages.

The FT-IR spectrum of PEI-3 shows N–H stretching at 3381 cm^{-1}, aliphatic C–H stretching at 2936 and 2828 cm^{-1}, and prominent imide C=O bands at 1689 and 1649 cm^{-1}, along with aromatic C=C vibrations at 1592 cm^{-1}. Additional C–N stretching bands are observed in the range of 1438–1272 cm^{-1}, while aromatic C–H bending modes associated with the perylene unit appear at 809 and 748 cm^{-1}. A similar spectral evolution is observed for PEI-5 (Fig. S3c), further confirming the successful formation of cross-linked polymer networks.

The ^{1}H NMR spectra further support the successful incorporation of perylene units into the polyethyleneimine framework and the formation of cross-linked PEI–perylene polymer networks (PEI-3 and PEI-5) (Figs. S4–S7). PEI was readily soluble in D_2O; however, the perylene-containing cross-linked polymers exhibited limited solubility in this solvent. Therefore, DMSO-d_6 was used as a suitable solvent for NMR analysis of both the starting PEI materials and the cross-linked products.

The ^{1}H NMR spectrum of PEI 60 kDa shows broad resonances in the region of 2.40–3.16 ppm, assigned to the methylene protons of the branched PEI backbone. In contrast, the NH/NH_2-related protons appear within the broad aliphatic envelope (Fig. S4). Similarly, PEI 25 kDa exhibits characteristic PEI backbone resonances in the range of 1.84–2.55 ppm, corresponding mainly to CH_2 protons adjacent to primary, secondary, and tertiary amine environments (Fig. S6). These broad signals are typical of branched PEI, where the different amine environments and polymeric structure lead to overlapping resonances.

After cross-linking with perylene-3,4,9,10-tetracarboxylic dianhydride, the spectra of PEI-3 and PEI-5 show a new broad aromatic resonance at approximately 8.01 ppm, which is assigned to the aromatic protons of the perylene core (Figs. S5 and S7). The appearance of this signal, which is absent in the starting PEI spectra, provides direct NMR evidence for the incorporation of the perylene unit into the polymer networks. In addition, the PEI backbone signals broaden and shift to broader chemical-shift regions after cross-linking. For PEI-3, the CH_2 proton signals are observed between 2.34 and 3.36 ppm, whereas for PEI-5 they extend from 1.91 to 3.48 ppm.

Compared with the starting PEI materials, these downfield shifts and broadening effects indicate changes in the local electronic environment of the PEI methylene and amine-containing segments, consistent with the formation of imide-linked PEI–perylene networks.

The combined appearance of the perylene aromatic proton resonance at ca. 8.01 ppm and the broadening/chemical-shift changes of the PEI backbone signals provide quantitative spectroscopic evidence for the successful incorporation of perylene moieties and the formation of cross-linked polymer networks. These NMR results are in good agreement with the FT-IR data, particularly the disappearance of the anhydride bands and the appearance of imide-related absorptions.

In addition, X-ray photoelectron spectroscopy (XPS) core-level measurements were conducted to gain further insights into the elemental composition and surface chemical characteristics of the PEI-3 and PEI-5 polymer networks (Fig. 2). The spectra exhibited distinct C 1s, N 1s, and O 1s signals, confirming the presence of carbon, nitrogen, and oxygen functionalities in both polymer matrices. Notably, the N 1s signal is particularly significant, as the perylene dianhydride precursor lacks nitrogen, suggesting successful incorporation of polyethylenimine (PEI) into the perylene-based network. Although peak deconvolution was not performed, the N 1s signal cannot be exclusively attributed to imide nitrogen; it is likely representative of nitrogen environments associated with both PEI-derived amines and imide functionalities. Alongside the Fourier-transform infrared spectroscopy (FTIR) findings—such as the vanishing of characteristic anhydride bands at 1773 and 1023 cm^{-1}, and the emergence of imide-related absorption peaks—combined with the nuclear magnetic resonance (NMR) results, the XPS data robustly corroborate the successful synthesis of imide-linked PEI–perylene polymer networks.

3.2. Optical properties

The optical properties of the perylene cross-linked polyethyleneimine networks (PEI-3, 60 kDa; PEI-5, 25 kDa) were investigated using UV–visible absorption and fluorescence spectroscopy. Both polymers exhibit limited solubility in polar solvents such as DMF, DMAc, NMP, DMSO, and acetic acid; therefore, their optical properties were analysed in these media (Fig. 3, Tables 1, S2 and S3).

View Article Online
DOI: 10.1039/D6MA00426A

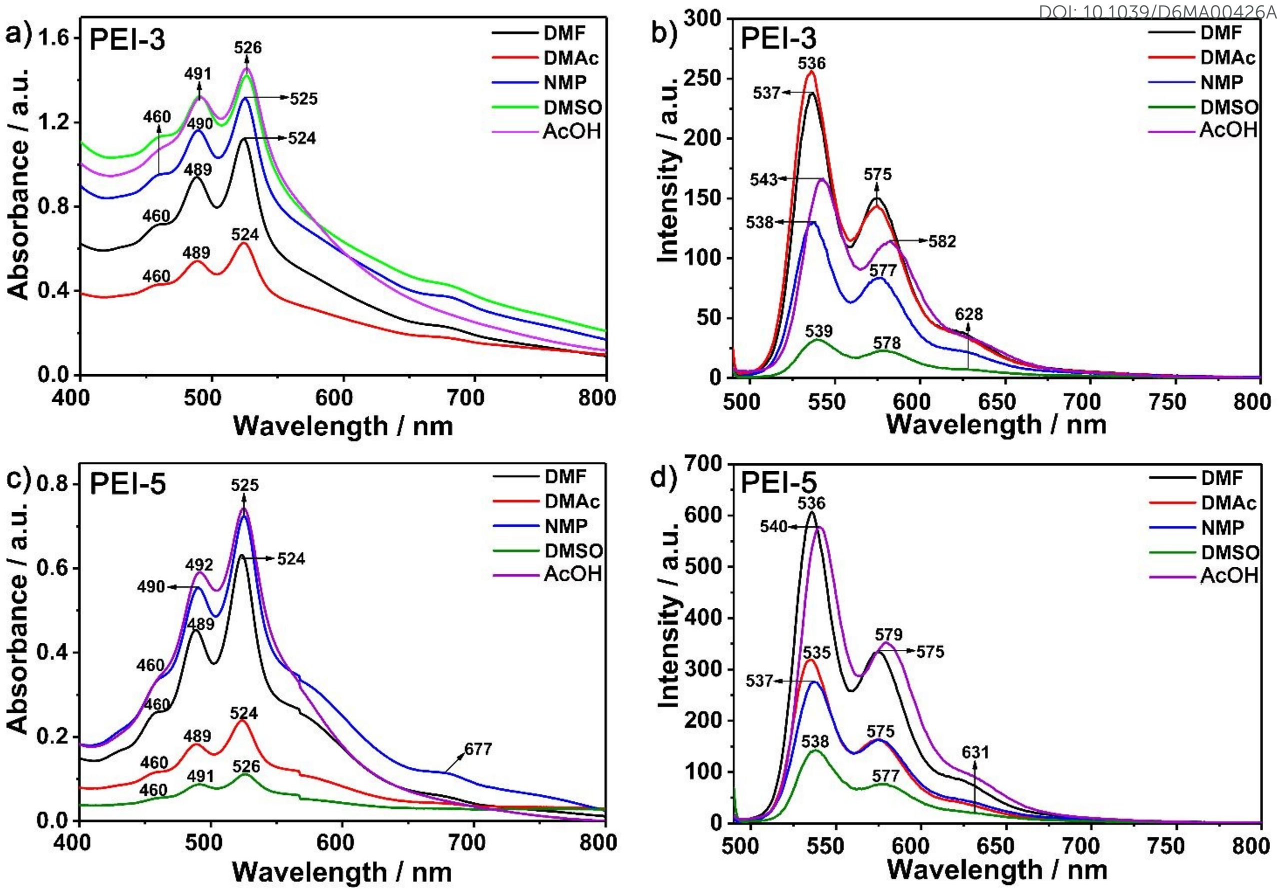

Fig. 3 UV–vis absorption spectra of (a) PEI-3 and (c) PEI-5, and fluorescence emission spectra of (b) PEI-3 and (d) PEI-5 in different solvents. The emission spectra were recorded upon excitation at $\lambda_{exc} = 485$ nm.

The UV–vis absorption spectra of PEI-3 and PEI-5 exhibit the characteristic vibronic progression of perylene chromophores, with three main absorption bands assigned to the 0–2, 0–1, and 0–0 transitions. The preservation of these vibronic bands in different polar solvents indicates that the perylene chromophore remains the dominant light-absorbing unit in both polymer networks. However, small variations in the relative vibronic intensities and peak positions reveal changes in the local aggregation environment of the perylene units. In perylene-based chromophores, the relative intensities of the 0–0 and 0–1 bands are commonly used as indicators of excitonic coupling and aggregation. A decrease in the A_{0-0}/A_{0-1} ratio is generally associated with stronger H-type aggregation, in which face-to-face π–π interactions attenuate the 0–0 transition and promote non-radiative decay pathways. Therefore, the observed changes in the vibronic profiles of PEI-3 and PEI-5 suggest different degrees of interchromophoric coupling within the cross-linked networks.

The solvent-dependent absorption and emission spectra further indicate that both polymers experience moderate solvatochromic effects. Slight bathochromic shifts in polar solvents

View Article Online
DOI: 10.1039/D6MA00426A

suggest stabilization of the excited state relative to the ground state, which is consistent with the presence of polar imide and amine-containing environments in the polymer networks. Nevertheless, the relatively small shifts observed across DMF, DMAc, NMP, DMSO, and AcOH indicate that the photophysical behaviour is governed not only by solvent polarity but also by aggregation, polymer-chain packing, and specific solvent–polymer interactions. In particular, AcOH may influence the spectra by partially protonating amine groups and altering polymer–solvent interactions. In contrast, highly polar aprotic solvents such as DMF, DMAc, NMP, and DMSO mainly affect the solvation and dispersion of the polymer networks.

The fluorescence spectra exhibit structured emission bands in the 535–700 nm region, characteristic of perylene-based emissive units. However, the low fluorescence quantum yields observed for both PEI-3 and PEI-5 indicate significant fluorescence quenching. This behaviour is consistent with aggregation-caused quenching commonly observed in perylene diimide/perylene-based systems, where strong π–π interactions facilitate exciton migration and non-radiative relaxation. Thus, the combined UV–vis and fluorescence results suggest that the PEI–perylene networks retain perylene-like optical signatures while displaying aggregation-mediated fluorescence quenching. These aggregation effects are also relevant to the electrochemical behaviour, since π–π interactions between perylene units can enhance electronic communication within the network. In contrast, excessive aggregation may reduce fluorescence and limit the accessibility of some electroactive sites.

The optical results also provide important insight into the electrochemical behaviour of the PEI–perylene polymer networks. The characteristic vibronic absorption bands and the low fluorescence quantum yields indicate strong intermolecular interactions between perylene chromophores, leading to aggregation-induced fluorescence quenching. Such aggregation behaviour is particularly relevant for electrochemical performance, because π–π interactions between perylene-imide units can facilitate electronic communication and charge delocalisation within the polymer network. Therefore, the optical signatures of aggregation are directly related to the charge-transport properties of the electrodes. In this context, PEI-5, which shows stronger aggregation-related optical features, is expected to possess a more electronically interconnected perylene framework, contributing to its improved rate capability, lower charge-transfer resistance, and enhanced cycling stability.

In contrast, PEI-3 exhibits a higher specific capacitance, attributed mainly to its more open, ion-accessible morphology, which allows more effective electrolyte penetration and the utilisation of redox-active sites. Thus, the optical and electrochemical data together suggest that PEI-3 benefits from morphological accessibility, whereas PEI-5 benefits from stronger π–π interactions and

View Article Online
DOI: 10.1039/D6MA00426A

electronic connectivity. This correlation explains the balance between capacitance, rate performance, and cycling stability in the two PEI–perylene polymer networks. In addition, the polymer solutions display solvatofluorochromism, showing a characteristic bordeaux colour under ambient light and bluish–yellow emission under UV irradiation (365 nm), as summarised in Table 1 and Fig. S8.

Table 1 Absorption wavelengths λ_{abs} (nm), maximum absorption wavelengths $\lambda_{abs,max}$ (nm), emission wavelengths at excitation 485 nm λ_{em} (nm), maximum emission wavelengths at excitation 485 nm $\lambda_{em,max}$ (nm) and Stokes shifts $\Delta\bar{\upsilon}$ (cm^{-1}) of PEI-3 and PEI-5 in various solvents.

	Solvent	λ_{abs}/nm	$\lambda_{abs,max}$/nm	$\lambda_{em}{}^{a}$/nm	$\lambda_{em,max}$/nm	$\Delta\bar{\upsilon}$/cm^{-1}
PEI-3	AcOH	526, 491, 460	526	543, 582, 628	543	595
	NMP	525, 490, 460	525	538, 577, 628	538	460
	DMF	524, 489, 460	524	537, 575, 628	537	462
	DMAc	524, 489, 460	524	536, 575, 628	536	427
	DMSO	526, 491, 460	526	539, 578, 628	539	458
PEI-5	AcOH	525, 492, 460	525	540, 579, 631	540	529
	NMP	525, 490, 460	525	537, 575, 631	537	426
	DMF	524, 489, 460	524	536, 575, 631	536	427
	DMAc	524, 489, 460	524	535, 575, 631	535	392
	DMSO	526, 491, 460	526	538, 577, 631	538	424

[a] λ_exc= 485 nm

3.3. Thermal stability of perylene cross-linked polyethyleneimine polymers

The thermal stability of the cross-linked polymers (PEI-3 and PEI-5) and their corresponding polyethyleneimine precursors (2 and 4) was evaluated by thermogravimetric analysis (TGA) at a heating rate of 10 °C min^{-1} over the temperature range of 25–900 °C (Fig. 4). All samples exhibit an initial weight loss below 130 °C, which is attributed to the removal of physically adsorbed and chemically bound water. The pristine polyethyleneimines exhibit typical thermal degradation behaviour, with PEI (2, 60 kDa) beginning to decompose at approximately 310 °C, accompanied by significant mass loss (~78%) and a negligible char residue (0.22%).

In contrast, the cross-linked polymer PEI-3 exhibits enhanced thermal resistance, with decomposition initiating at around 270 °C and a more gradual mass loss (45%) over 270–543 °C. This behaviour results in a slightly higher char yield (0.72%) than that of the unmodified

View Article Online
DOI: 10.1039/D6MA00426A

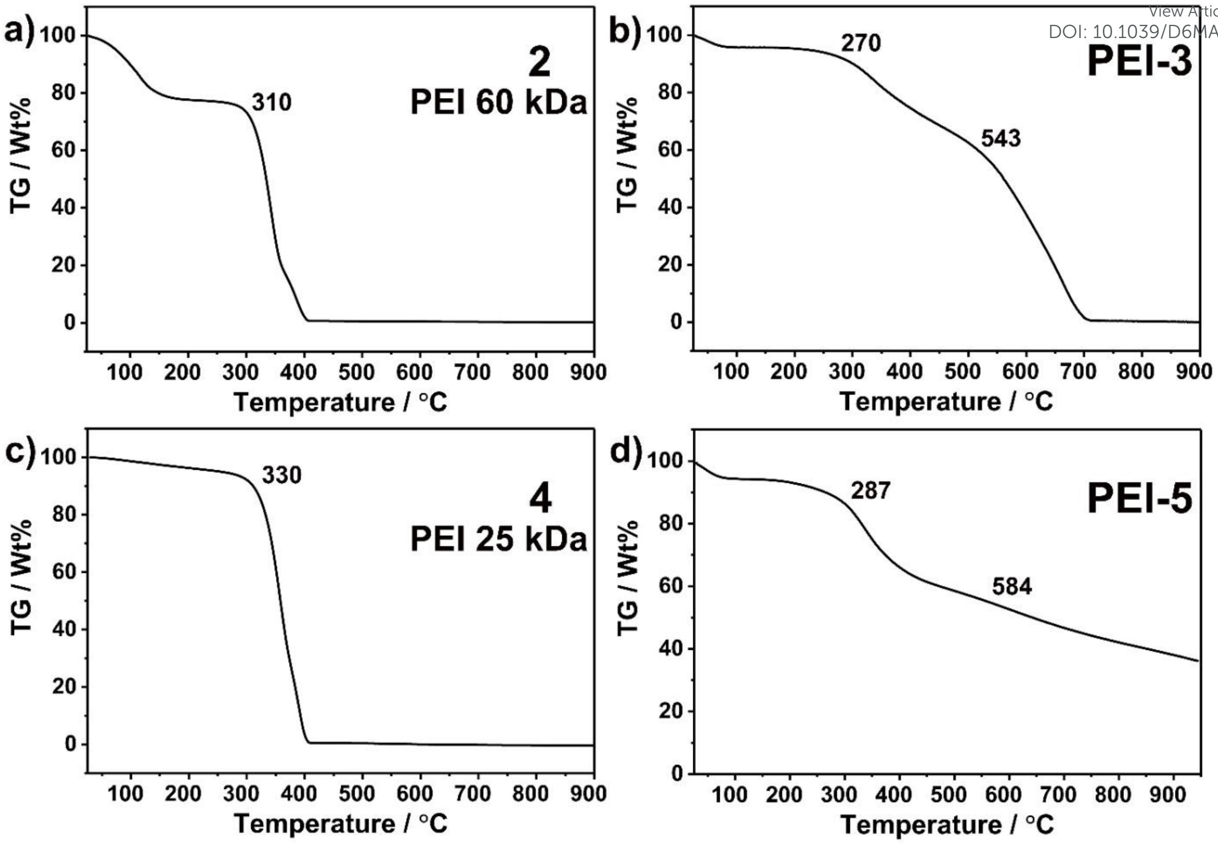

Fig. 4 TGA curves of (a) PEI 60 kDa, (b) PEI-3, (c) PEI 25 kDa, and (d) PEI-5 recorded at a heating rate of 10 °C min^{-1} under nitrogen atmosphere.

polymer (2). For the lower-molecular-weight polyethyleneimine (4, 25 kDa), thermal degradation begins at approximately 330 °C, with similar mass loss and char yields to those of polyethyleneimine (2, 60 kDa). Notably, the corresponding cross-linked polymer PEI-5 shows improved thermal performance, with decomposition starting at 287 °C and a significantly higher char yield (36.14%) at 950 °C. Moreover, PEI-5 maintains structural integrity over a broader temperature range, indicating increased resistance to thermal degradation. Overall, the cross-linked polymers exhibit greater thermal stability and char-forming ability than their linear counterparts. The improved thermal behaviour is attributed to the incorporation of rigid, π-conjugated perylene units and the formation of a cross-linked network, which restricts chain mobility and promotes carbonaceous residue formation at elevated temperatures. The higher char yield observed for PEI-5 compared to PEI-3 suggests differences in network architecture and cross-linking density. This may be associated with reduced steric hindrance and more efficient packing in PEI-5, thereby improving thermal stability.

These findings demonstrate the crucial role of π-conjugated cross-linking in enhancing thermal stability and char formation, suggesting that these materials hold significant potential for high-temperature and advanced energy storage applications.

View Article Online
DOI: 10.1039/D6MA00426A

3.4. Morphological Characterisation

The morphological, elemental, and structural properties of the polymer-based electrode coatings deposited on graphite substrates were investigated using SEM, EDX, Raman spectroscopy, and TEM (Figs. 5 and S9). SEM images (Figs. 5a and 5b) reveal clear morphological differences between PEI-3 and PEI-5.

PEI-3 exhibits a more open, wrinkled, and void-rich morphology with interconnected surface features, whereas PEI-5 shows a more compact and layered morphology with denser polymer packing. Based on image-based SEM/TEM observations, PEI-3 contains larger and more interconnected void-like regions, while PEI-5 displays smaller and less accessible interparticle/interlayer spaces. Since gas adsorption-based BET surface area and pore-size distribution measurements were not available, the morphology is discussed here in terms of semi-quantitative image-derived structural features rather than quantitatively defined pore-size distribution.

EDX analysis (Figs. 5c and 5d) confirms that both materials are mainly composed of carbon, nitrogen, and oxygen. The elemental composition of PEI-3 was determined as C 79.6 at%, N 12.7 at%, and O 7.7 at%, while PEI-5 exhibits C 78.1 at%, N 12.1 at%, and O 9.7 at%, indicating comparable elemental compositions for both polymer networks.

The baseline-corrected Raman spectra (Figs. 5e and 5f) further support the presence of the perylene-based conjugated framework. PEI-3 displays characteristic bands at 1297, 1380, and 1576 cm^{-1}, while PEI-5 shows corresponding bands at 1293, 1377, and 1576 cm^{-1}. The bands at 1380 cm^{-1} for PEI-3 and 1377 cm^{-1} for PEI-5 are assigned to D-like bands associated with disordered aromatic/sp^2 carbon domains and skeletal vibrations of the perylene-based framework, whereas the band at 1576 cm^{-1} corresponds to a G-like band related to aromatic sp^2 C=C stretching vibrations. The additional bands at 1297 and 1293 cm^{-1} are attributed to perylene skeletal/C–N-related vibrational modes within the cross-linked polymer networks.

View Article Online
DOI: 10.1039/D6MA00426A

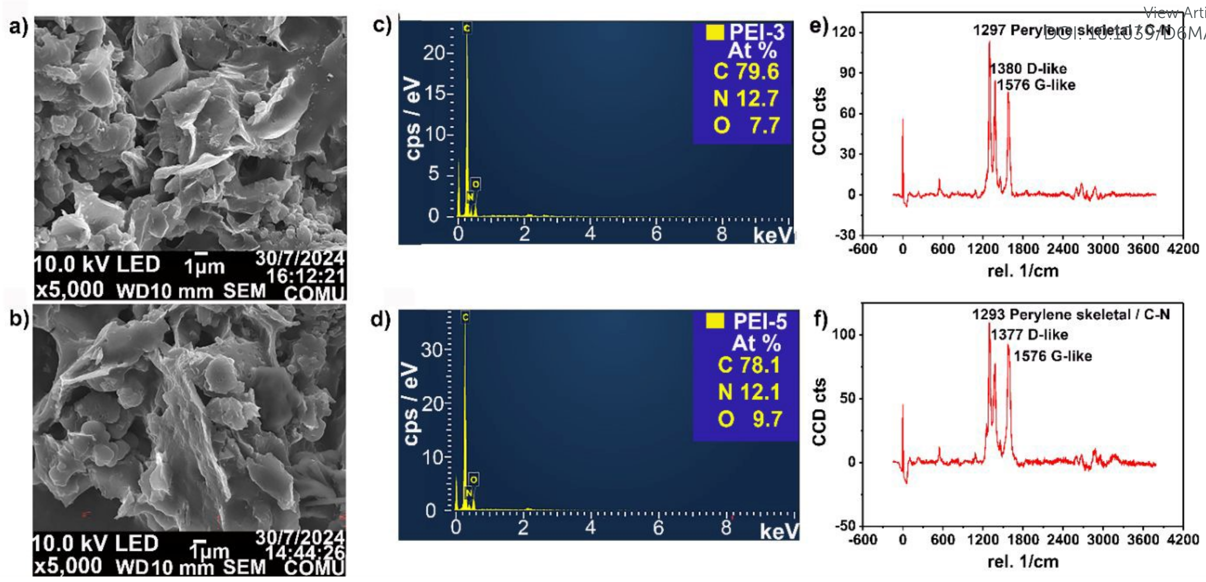

Fig. 5 SEM images of (a) PEI-3 and (b) PEI-5, corresponding EDX spectra of (c) PEI-3 and (d) PEI-5, and baseline-corrected Raman spectra of (e) PEI-3 and (f) PEI-5. The Raman bands assigned to perylene skeletal/C–N vibrations and D-like and G-like bands are indexed.

TEM images (Fig. S9) are consistent with the SEM observations. PEI-3 exhibits a heterogeneous, relatively open network morphology with interconnected contrast variations and void-like regions, suggesting improved electrolyte accessibility. In contrast, PEI-5 exhibits a more compact, layered structure, consistent with a denser packing of the polymer network. These image-based morphological differences help explain the electrochemical behaviour of the two materials: the more open and ion-accessible morphology of PEI-3 favours electrolyte penetration and the utilisation of redox-active sites, whereas the denser structure of PEI-5 may restrict ion diffusion but can provide improved structural integrity and electronic connectivity.

3.5. Electrochemical characterisation and supercapacitor (SC) performances of PEI-3 and PEI-5

The electrochemical investigations demonstrate that the cross-linking of perylene with polyethyleneimine (PEI) significantly impacts both the charge-storage mechanism and the overall electrochemical performance of the resultant hybrid material (Fig. 6). The condensation reaction involving Perylene-3,4,9,10-tetracarboxylic dianhydride in conjunction with either branched polyethyleneimine precursors leads to the formation of structures that exhibit varying topological characteristics. The branched PEI-3 showed increased porosity, facilitating enhanced hybrid ion diffusion. At the same time, the PEI-5 exhibited a higher cross-link density and a more conjugated structure, resulting in superior electronic interconnectivity through effective π-π stacking of the perylene units. As illustrated in Fig. 6a and 6b, both materials exhibited characteristics of electric double-layer capacitance and pseudo-capacitance in their cyclic voltammetry (CV) profiles. The quasi-rectangular CV envelopes and the redox peaks observed between 0.3 and 0.6 V (vs Ag/AgCl) indicate rapid Faradaic surface redox reactions on the perylene-imide moieties.

These findings were further validated by the galvanostatic charge-discharge (GCD) curves presented in Fig. 6c and d, which exhibited a nearly symmetrical triangular shape, minimal IR drop, and excellent reversibility. The specific capacitance of PEI-3 was higher than that of PEI-5, measuring 343.7 F g^{-1} at 1 A g^{-1} compared to 185.2 F g^{-1} for PEI-5 at the same low current densities. As is typical with supercapacitor cells, the specific capacitance decreased with increasing current density, dropping to 250.3 F g^{-1} for polymer PEI-3 and 123.3 F g^{-1} for polymer PEI-5 at 6 A g^{-1}. Notably, PEI-5 demonstrated greater capacitance retention during high-rate cycling. In perylene-diimide-based conjugated systems, electrochemical performance is widely reported to be closely related to charge delocalisation and intermolecular interactions (Table S4). Specifically, the 2D conjugated structure of the perylene core supports rapid redox kinetics by enabling more efficient charge transport along the molecular backbone and intermolecularly. The more porous, ion-accessible morphology of PEI-3 enables electrolyte ions to reach redox-active sites more readily, resulting in higher capacitive behaviour.

In contrast, the more compact and ordered structure of PEI-5 creates stronger stacking interactions and more integrated charge-transport pathways, enhancing cycle and charge-transfer stability. This behavior is consistent with previous studies reporting that charge transport and redox activity in perylene-based conjugated polymers are controlled by both morphological accessibility and electronic connectivity (Table S4). The observed stability in the system can be attributed to its compact, cross-linked framework, which facilitates rapid ion movement and efficient electron transport through a well-connected conjugated backbone. Further analysis of capacitance contributions using Dunn's method corroborates this behaviour (Fig. 6e, f). The charge-storage behavior of both PEI-3 and PEI-5 arises from the combined contribution of electric double-layer capacitance (EDLC) and pseudocapacitance. The EDLC contribution mainly arises from electrostatic ion adsorption/desorption at the porous electrode/electrolyte interface, while the pseudocapacitive behaviour is associated with rapid, reversible faradaic redox reactions at the perylene-imide moieties and nitrogen-containing functional groups within the polymer backbone. The coexistence of quasi-rectangular CV profiles and broad redox peaks confirms the hybrid charge-storage mechanism in both systems. In both examined systems, a notable increase in the pseudocapacitive contribution was observed at higher scan rates,

View Article Online
DOI: 10.1039/D6MA00426A

indicating a fast, surface-controlled charge-storage mechanism. Notably, the PEI-5 consistently exhibited a greater pseudocapacitive contribution across all scan rates, indicating enhanced utilisation of electroactive sites and superior charge-transfer dynamics. These findings underscore the significance of minor structural variations in the amine precursor that influence the interplay between the electric double-layer and Faradaic contributions. Although the branched PEI-3 exhibits a higher charge-storage capacity due to its accessible redox-active amines and porous architecture, the linear PEI-5 demonstrates improved rate capability and cycling stability, owing to its densely integrated electronic perylene framework. To evaluate the electrochemical kinetics in more detail, b-value analysis was performed (Fig. S10). The calculated b-values were approximately 0.65 and 0.52 for the PEI-3 and PEI-5 electrodes, respectively. The higher b-value obtained for PEI-3 indicates that the surface-controlled capacitive contribution is more dominant in the charge storage mechanism and that charge transfer kinetics are faster. In contrast, the b-value of approximately 0.52 for PEI-5 indicates that diffusion-controlled processes more strongly influence the electrochemical behaviour. These results support the idea that the porous, ion-accessible structure of PEI-3 enables more efficient ion transport, whereas ion diffusion remains relatively limited in PEI-5 due to its more compact morphology.

Further insight into the electrochemical behaviour of PEI-3 and PEI-5 is provided in Fig.7. The CV and GCD profiles (Figs. 7a and 7b) reveal distinct charge-storage characteristics for the two materials. PEI-3 exhibits higher current response and longer discharge times, attributed to its porous network structure, which enhances ion transport and utilises electroactive sites more effectively. In contrast, PEI-5 displays more rectangular CV curves and highly symmetric GCD profiles with a reduced IR drop, indicating improved charge–discharge kinetics and enhanced electronic conductivity. These observations suggest that the compact and more interconnected structure of PEI-5 facilitates efficient electron transport.

View Article Online
DOI: 10.1039/D6MA00426A

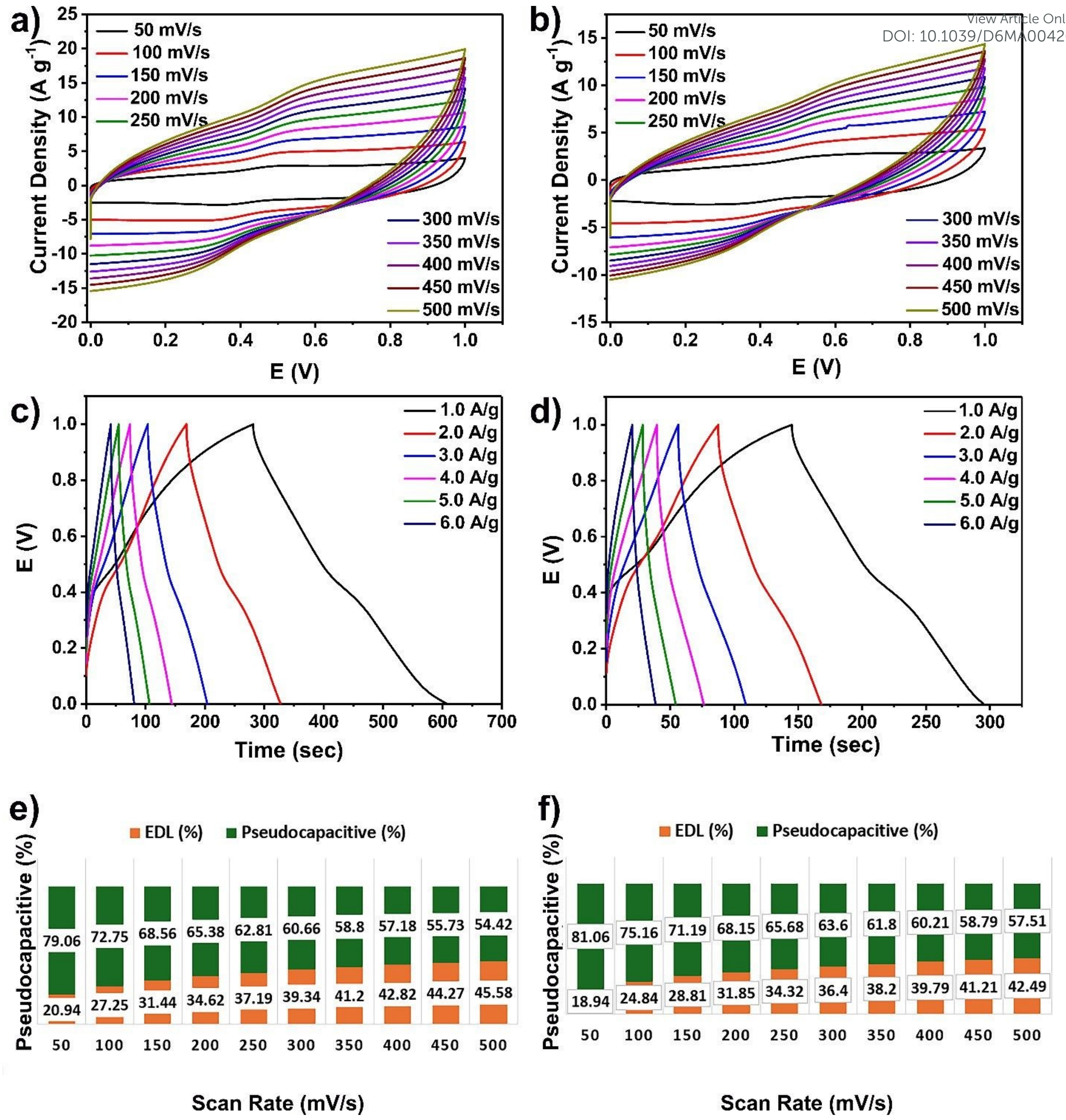

Fig. 6 Electrochemical performance of PEI-3 and PEI-5 electrodes: CV curves of (a) PEI-3 and (b) PEI-5 recorded at scan rates of 50–500 mV s^{-1}; GCD profiles of (c) PEI-3 and (d) PEI-5 measured at different current densities; and capacitive contribution analysis of (e) PEI-3 and (f) PEI-5 showing the electric double-layer and pseudocapacitive contributions at different scan rates.

Electrochemical impedance spectroscopy (EIS) analysis (Fig. 7c) further elucidates the interfacial properties of the electrodes. PEI-3 exhibits a smaller intercept in the high-frequency region and a steeper slope in the low-frequency region, indicative of lower internal resistance and more ideal capacitive behaviour. This is consistent with its porous morphology, which promotes electrolyte penetration and efficient ion diffusion. In comparison, PEI-5 shows a slightly higher overall impedance and a less pronounced slope, reflecting increased charge-transfer resistance and reduced ion mobility due to its denser microstructure. Furthermore, the EIS spectra were fitted using an equivalent circuit model comprising the solution resistance (Rs), a constant phase element (CPE), the charge-transfer resistance (Rct), and a Warburg diffusion element (W). The CPE was used instead of an ideal capacitor to account for the non-ideal capacitive behavior arising from surface heterogeneity and porous electrode morphology. The fitted results revealed that PEI-3 exhibited lower charge-transfer resistance and improved ion-diffusion behavior compared to PEI-5, indicating more efficient electrolyte penetration and faster interfacial charge-transfer kinetics. These findings are consistent with the CV and GCD results and highlight the structure-dependent electrochemical behaviour of the materials. While the porous architecture of PEI-3 favours ion transport and high capacitance, the more compact structure of PEI-5 enhances electronic conductivity and structural stability.

The rate capability and cycling stability of the electrodes are summarised in Fig. 8. As expected, both materials exhibit a decrease in specific capacitance with increasing current density due to diffusion limitations at higher rates. However, PEI-3 consistently delivers higher capacitance across all current densities, reflecting its enhanced ion accessibility and higher electroactive site density.

Long-term cycling tests demonstrate that PEI-3 retains approximately 83% of its initial capacitance after 6000 cycles, compared to 71% for PEI-5. This indicates that the open, porous structure of PEI-3 more readily accommodates repeated ion insertion and extraction.

The differences in electrochemical performance can be rationalised on structural grounds. PEI-3, with its more extended and porous architecture, provides a greater number of accessible redox-active sites, resulting in enhanced pseudocapacitive behaviour. However, this structure may introduce longer ion diffusion pathways at higher current densities. In contrast, PEI-5 forms a more compact, densely cross-linked network, reducing steric hindrance and enhancing structural integrity, thereby improving rate capability and cycling stability.

This behaviour is consistent with previous reports on perylene-based conjugated systems, in which the balance among porosity, cross-linking density, and electronic connectivity plays a critical role in determining electrochemical performance [43].

View Article Online
DOI: 10.1039/D6MA00426A

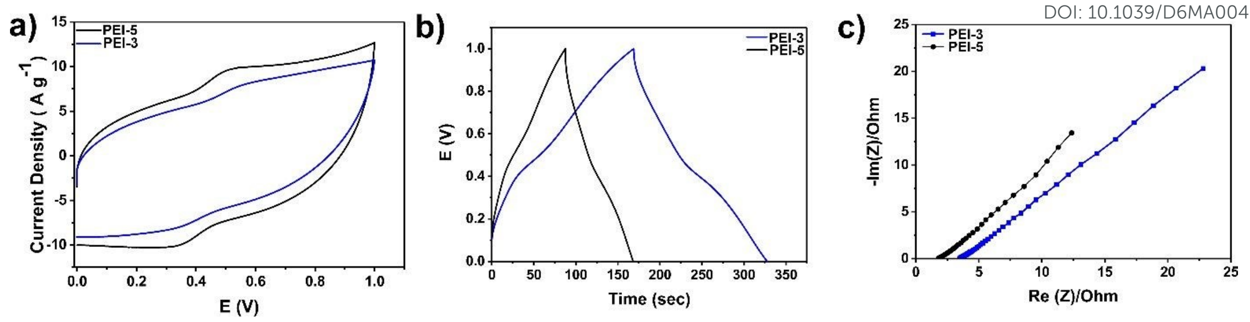

Fig. 7 Comparative electrochemical behaviour of PEI-3 and PEI-5 electrodes: (a) CV curves recorded at a scan rate of 300 mV s^{-1}, (b) GCD curves measured at a current density of 2 A g^{-1}, and (c) EIS Nyquist plots.

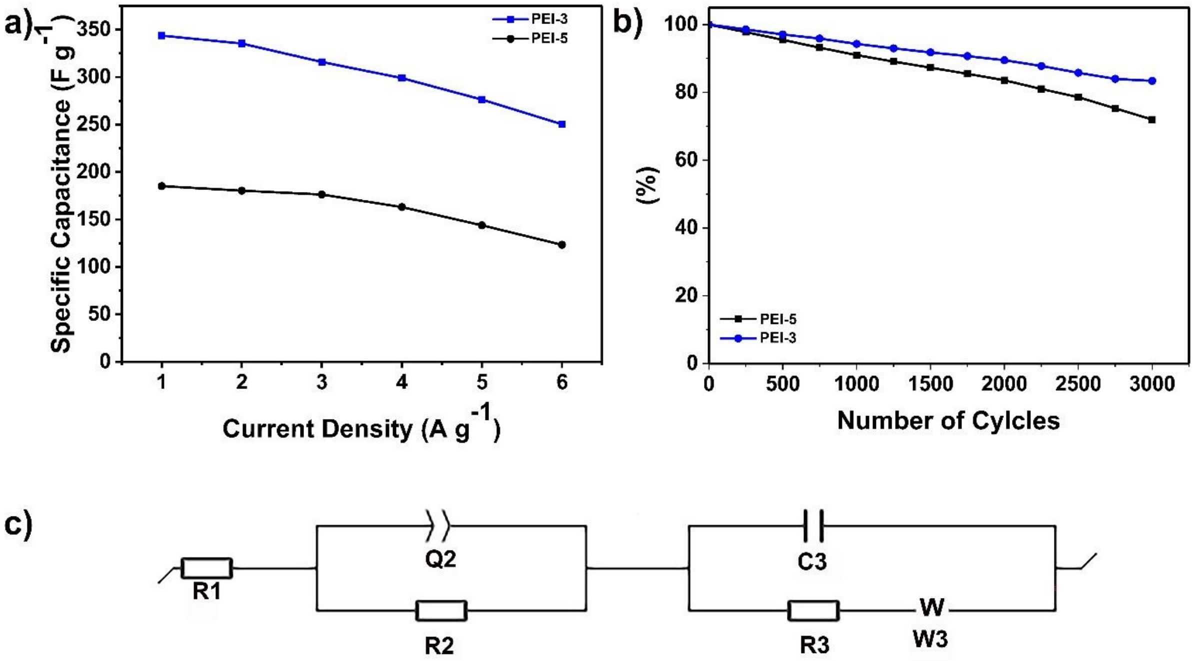

Fig. 8 (a) Specific capacitance of PEI-3 and PEI-5 electrodes at different current densities; (b) where the balance between porosity, cross-linking density, and electronic connectivity plays a role in the cycling stability of PEI-3 and PEI-5 electrodes over 3000 charge-discharge cycles, and (c) an equivalent circuit model to analyse the EIS response.

When the CV and GCD curves obtained at different potential windows are examined in Figure S11, it is seen that the device largely maintains its electrochemical stability up to 1.7 V. At higher potential ranges, distortions in the CV curves and significant deviations in the GCD curves appear, indicating the onset of electrolyte degradation and side reactions. Therefore, the optimum operating potential range for the symmetrical device has been determined as 0.0-1.7 V. Thanks to its semi-branched and porous structure, the improved electrochemical performance of the PEI-3 electrode compared to PEI-5 was evaluated in detail using a symmetrical supercapacitor device and its full cell performance (Figs. 9 and 10). The CV

View Article Online
DOI: 10.1039/D6MA00426A

curves show that the curves largely maintain their semi-rectangular form and offer a wide field of view throughout the scan rates of 50-500 mV s^{-1} (Fig. 9a). Furthermore, the persistence of redox doping even at high scan rates indicates that the perylene diimide centers in the PEI-3 structure actively participate in fast and reversible faradaic reactions. The shape of the curves, especially at high scan rates, indicates that the electrode's ion transport mechanism is largely pseudo-capacitive. The GCD curves obtained at different current densities exhibit a highly symmetrical triangular profile and an IR drop of approximately 0.1 V (Fig. 9b). This indicates that the device exhibits high reversibility and improved charge-transfer kinetics. Furthermore, longer discharge times at lower current densities, such as during a high operating window of 1.8 V, support the device's high charge storage capacity. The specific capacitance values of the symmetrical device are given in Fig. 9c. The PEI-3-based device exhibits a specific capacitance of 107 F g^{-1} at a current density of 1 A g^{-1}, while the capacitance drops to 42.1 F g^{-1} when the current density increases to 5 A g^{-1}. This decrease can be attributed to the insufficient diffusion of electrolyte ions into the active sites at high current densities. However, the device's ability to maintain significant capacitive behavior even at high currents indicates that the structure is suitable for fast charge-discharge applications. Furthermore, throughout the cyclic test, the Coulomb efficiency remained between 88% and 93%, demonstrating the device's high reversibility and stable charge-discharge behaviour (Fig. S12). The Ragone plot reveals the relationship between energy and power density of the device (Fig. 9d). Higher energy density is achieved at lower power densities.

In contrast, energy density gradually decreases as power density increases. The PEI-3-based symmetrical device delivered a maximum energy density of 43 Wh kg^{-1} at a power density of 850.7 W kg^{-1} at a current density of 1 A g^{-1}. This behaviour is typical of hybrid supercapacitor systems and demonstrates that the PEI-3-based device can provide both high energy storage capacity and fast power output. The cycle stability plot shows that the PEI-3 symmetrical device retains 81% of its initial capacitance after 4000 charge-discharge cycles (Fig. 9e). The limited capacitance loss indicates that the porous, ion-accessible structure of PEI-3 maintains its structural integrity over long cycles. This demonstrates that the electrode structure is resistant to repeated ion input-output processes (Figs. 9 and 10).

View Article Online
DOI: 10.1039/D6MA00426A

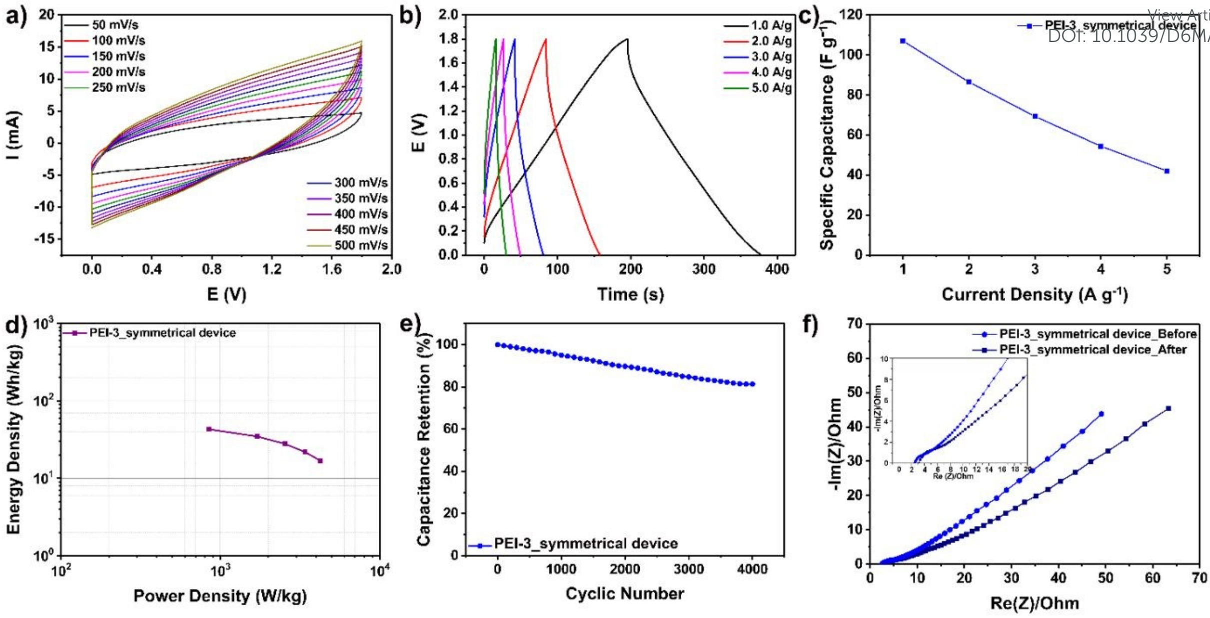

Fig. 9 Electrochemical performance of the PEI-3 symmetric supercapacitor device: (a) CV curves recorded at scan rates of 50–500 mV s⁻¹, (b) GCD profiles measured at different current densities, (c) specific capacitance as a function of current density, (d) Ragone plot, (e) cycling stability over 4000 charge–discharge cycles, and (f) EIS Nyquist plots recorded before and after the cycling stability test.

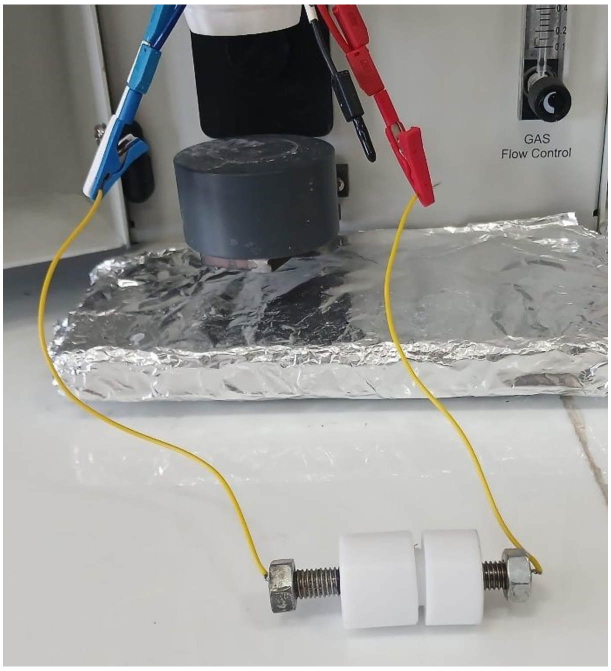

Fig. 10 Photograph of the assembled PEI-3 symmetric supercapacitor device used for electrochemical testing.

Finally, the EIS Nyquist curves show changes in electrochemical resistance before and after the cycle (Fig. 9f). Although a slight increase in resistance is observed in the post-cycle curves, the capacitive behaviour in the low-frequency region is largely preserved. This result

View Article Online
DOI: 10.1039/D6MA00426A

demonstrates that no significant degradation occurs at the electrode/electrolyte interface even after prolonged cycling, and the device maintains its electrochemical stability.

Overall, the PEI-3-based symmetrical supercapacitor device stands out as a promising energy storage system with its high capacitance, good cycling stability, and satisfactory energy-to-power performance.

4. Conclusion

In this study, two novel PEI–perylene polymer networks, PEI-3 and PEI-5, were successfully synthesised via imidization of branched polyethyleneimine with perylene-3,4,9,10-tetracarboxylic dianhydride. To the best of our knowledge, this is the first report of the use of perylene dianhydride as a π-conjugated cross-linking agent for PEI-based polymer networks. This strategy enables the integration of nitrogen-rich PEI segments with redox-active, π-conjugated perylene units within an insoluble, cross-linked architecture.

Spectroscopic and surface analyses confirmed the successful incorporation of perylene units and the formation of imide-linked polymer networks. The disappearance of anhydride-related FTIR bands, the appearance of imide absorptions, the perylene aromatic resonance in the ^{1}H NMR spectra, and the C 1s, N 1s, and O 1s XPS signals collectively support the proposed PEI–perylene network structure. The materials also exhibited reduced water solubility, characteristic perylene-based optical behavior, and improved thermal stability compared with the parent PEI precursors. Electrochemical measurements demonstrated that polymer architecture strongly influences charge-storage behavior. PEI-3 exhibited higher specific capacitance and better capacitance retention than PEI-5 over 3000 charge–discharge cycles, which is attributed to its more open, ion-accessible morphology. PEI-5, on the other hand, displayed greater thermal robustness and a more compact network structure, suggesting that the lower-molecular-weight PEI precursor promotes denser packing and improved structural integrity, although this compact morphology limits ion accessibility and reduces capacitance. Importantly, the PEI-3 symmetric supercapacitor device delivered a specific capacitance of 107 F g^{-1} at 1 A g^{-1}, a maximum energy density of 43 Wh kg^{-1} at a power density of 850.7 W kg^{-1}, and retained 81% of its initial capacitance after 4000 cycles. The EIS results recorded before and after cycling further indicate that the capacitive behaviour is largely preserved, despite a slight increase in resistance.

View Article Online
DOI: 10.1039/D6MA00426A

Overall, this work establishes perylene dianhydride cross-linking as a promising molecular design strategy for developing nitrogen-rich, redox-active, metal-free polymer networks. These findings offer valuable insight into the design of π-conjugated organic electrode materials for advanced supercapacitor applications.

CRediT authorship contribution statement

Huriye Icil: Conceptualisation, data curation, formal analysis, investigations, methodology, supervision, resources, project administration, visualisation, writing – review & editing. **Pelin Karsili:** Investigation, data curation. **Meltem Dinleyici:** Investigation, visualisation, data curation. **Jahan Tohtayeva:** Data curation**. Sinem Altınışık:** Investigation, visualisation, data curation. **Sermet Koyuncu:** Data curation, Writing – review & editing.

Declaration of Competing Interest

The authors declare that they have no known competing financial interests or personal relationship that could have influenced the work reported in this paper.

Acknowledgment

The support from Eastern Mediterranean University Research Funding (BAPC-04-21-03) is acknowledged.

Appendix A. Supplementary material

Supplementary data to this article can be found online at https://doi. org/.

Data availability

Data will be made available on request.

References

[1] A. Shamoon, A. Haleem, S. Bahl, M. Javaid and S. B. Garg, Mater. Today Proc., 2022, 62, 63–69.

View Article Online
DOI: 10.1039/D6MA00426A

[2] W. S. Ebhota and T. C. Jen, Int. J. Precis. Eng. Manuf. Green Technol., 2020, 7, 97–117.

[3] A. Kalair, N. Abas, M. S. Saleem, A. R. Kalair and N. Khan, Energy Storage, 2021, 3, 1–27.

[4] Global Market Insights, Supercapacitor Market Size, Share & Forecast Analysis, 2025–2034, Report ID: GMI3732, 2025.

[5] P. Simon and Y. Gogotsi, Nat. Mater., 2008, 7, 845–854.

[6] J. Wang, Y. Xu, F. Yan, J. Zhu and J. Wang, J. Power Sources, 2011, 196, 2373–2379.

[7] G. H. Lee, J. W. Lee, J. I. L. Choi, S. J. Kim, Y. H. Kim and J. K. Kang, Adv. Funct. Mater., 2016, 26, 5139–5148.

[8] A. Dutta, S. Mitra, M. Basak and T. Banerjee, Energy Storage, 2023, 5, 1–36.

[9] N. Parvin, D. Merum, M. Kang, S. W. Joo, J. H. Jung and T. K. Mandal, J. Mater. Chem. A, 2025, 13, 24320–24386.

[10] E. M. Szumska, Energies, 2025, 18, 2422.

[11] L. Guo, P. Hu and H. Wei, J. Energy Storage, 2023, 65, 107269.

[12] N. Salah, M. Shehab, J. El Nady, S. Ebrahim, E. M. El-Maghraby and A. H. Sakr, Electrochim. Acta, 2023, 449, 142174.

[13] E. Vessally, R. M. Rzayev, A. A. Niyazova, T. Aggarwal and K. E. Rahimova, RSC Adv., 2024, 14, 40141–40159.

[14] K. Singh, Abhimanyu, S. Sonu, V. Chaudhary, P. Raizada, S. Rustagi, P. Singh, P. Thakur, V. Kumar and A. Kaushik, Adv. Colloid Interface Sci., 2024, 332, 103273.

[15] S. Subramanyam, Suman, L. Phor, V. Chaudhary, A. Kumar, P. Thakur, V. Kumar, K. Singh and A. Kaushik, J. Energy Storage, 2024, 92, 112043.

[16] Abhimanyu, K. Singh, H. Sable, Sonu, V. Kumar, P. Singh, A. Kaushik, P. Thakur and V. Chaudhary, Mater. Today, 2025, 90, 681–705.

View Article Online
DOI: 10.1039/D6MA00426A

[17] V. Chaudhary, J. Electrochem. Soc., 2025, 172, 017501.

[18] N. A. Salleh, S. Kheawhom, N. A. A. Hamid, W. Rahiman and A. A. Mohamad, J. Mater. Res. Technol., 2023, 23, 3470–3491.

[19] S. Sharma and P. Chand, Results Chem., 2023, 5, 100885.

[20] S. Ermis, S. Altinisik, F. Catoglu, Y. Yagci, E. Sari, S. Jockusch, S. Koyuncu and K. Kaya, Adv. Electron. Mater., 2025, 11.

[21] R. Lakra, R. Kumar, P. K. Sahoo, D. Thatoi and A. Soam, Inorg. Chem. Commun., 2021, 133, 108929.

[22] C. C. Chao, M. K. Leung, Y. O. Su, K. Y. Chiu, T. H. Lin, S. J. Shieh and S. C. Lin, J. Org. Chem., 2005, 70, 4323–4331.

[23] S. Hosseini, C. Madden, J. Hihath, S. Guo, L. Zang and Z. Li, J. Phys. Chem. C, 2016, 120, 22646–22654.

[24] A. De Adhikari, A. Morag, J. Seo, J. M. Kim and R. Jelinek, ChemSusChem, 2020, 13, 3230–3236.

[25] M. B. Miltenburg, S. Y. An, N. K. Obhi, E. Grignon, B. T. McAllister and D. S. Seferos, ACS Appl. Polym. Mater., 2020, 2, 5574–5580.

[26] P. Dubey, K. Bhardwaj, R. Kumar, S. Sundriyal and P. H. Maheshwari, J. Energy Storage, 2022, 56, 106058.

[27] M. R. Biradar, A. M. Kale, B. C. Kim, S. V. Bhosale and S. V. Bhosale, Energy Technol., 2022, 10, 2200154.

[28] L. Jiao, Z. Hu, F. Ma, Y. He, Q. Zhou, L. Xiao, L. Lv and Y. Yang, J. Energy Storage, 2022, 52, 104777.

[29] P. N. Singh, M. G. Mohamed, S. V. Chaganti, S. U. Sharma, M. Ejaz, J. T. Lee and S. W. Kuo, ACS Appl. Energy Mater., 2023, 6, 8277–8287.

[30] S. D. Jagdale, C. R. K. Rao, S. V. Bhosale and S. V. Bhosale, Chem. Eng. J. Adv., 2023, 14, 100499.

[31] S. H. Goudar, S. Bhoi, S. K. Sahoo, K. V. Rao and N. Kurra, Small, 2024, 20, 2309905.

[32] S. K. Pati, D. Patra, S. Muduli, S. Mishra and S. Park, J. Mater. Chem. A, 2024, 12, 21165–21175.

[33] S. D. Jagdale, C. R. K. Rao, S. V. Bhosale and S. V. Bhosale, J. Energy Storage, 2024, 90, 111874.

[34] V. Vinita, K. Surana, M. Guin, S. S. Soni and G. Durga, Dyes Pigm., 2025, 232, 112485.

[35] B. Al-Khateeb, M. Dinleyici, A. Abourajab, C. Kök, J. B. Bodapati, D. Uzun, S. Koyuncu and H. Icil, J. Photochem. Photobiol. A Chem., 2020, 393, 112432.

[36] M. Dinleyici, B. Al-Khateeb, A. Abourajab, D. Uzun, S. Koyuncu and H. Icil, J. Photochem. Photobiol. A Chem., 2021, 421, 113525.

[37] I. Yucekan, M. Dinleyici, S. Temurlu, R. Rashid, J. B. Bodapati, B. Al-Khateeb, A. Abourajab, P. Karsili, S. Altınışık, S. Koyuncu and H. Icil, Eur. Polym. J., 2023, 196.

[38] S. Temurlu, M. A. A. Abureesh, A. Abourajab, P. Karsili, M. Dinleyici, S. Altınışık, S. Koyuncu and H. Icil, Macromol. Res., 2024, 32, 281–297.

[39] M. A. Ghriga, B. Grassl, M. Gareche, M. Khodja, S. E. I. Lebouachera, N. Andreu and N. Drouiche, Polym. Bull., 2019, 76, 6001–6029.

[40] J. Wang, D. Jiang, Y. Zhang, Y. Du, Y. Sun, M. Jiang, J. Xu and J. Liu, J. Colloid Interface Sci., 2024, 653, 229–237.

[41] V. Vinita, P. S. Dhapola, M. Guin, P. K. Singh and G. Durga, J. Power Sources, 2025, 641, 236781.

[42] V. Vinita, M. Guin and G. Durga, ACS Appl. Electron. Mater., 2025, 7, 3230–3243.

[43] C. Wang, K. Hu, Y. Liu, M. R. Zhang, Z. Wang and Z. Li, Materials, 2021, 14, 1955.

[44] C. Liu, W. Yue, Y. Li and A. Huang, Chem. Eur. J., 2021, 27, 4876–4882.

View Article Online
DOI: 10.1039/D6MA00426A

Data availability

"The data that support the findings of this study are available from the corresponding author upon reasonable request."